

The Early Angular Momentum History of Low Mass Stars: Evidence for a Regulation Mechanism

L. M. Rebull^{1,2}, S. C. Wolff³, S. E. Strom³, R. B. Makidon⁴

ABSTRACT

We examine the early angular momentum history of stars in young clusters via 197 photometric periods in fields flanking the Orion Nebula Cluster (ONC), 81 photometric periods in NGC 2264, and 202 measurements of $v \sin i$ in the ONC itself. We show that PMS stars spanning an age range from 0.1 to 3 Myr do not appear to conserve stellar angular momentum as they evolve down their convective tracks, but instead preserve the same range of periods even though they have contracted by about a factor of three. This result seems to require a mechanism that regulates the angular velocities of young stars. We discuss several candidate mechanisms. The most plausible appears to be disk-locking, though most of our stars do not have $I_C - K_s$ excesses suggestive of disks. However, a decisive test of this hypothesis requires a more sensitive diagnostic than the $I_C - K_s$ excesses used here.

Subject headings: stars: pre-main sequence — stars: rotation

1. Introduction

Observations over the past decade have established that pre-main sequence (PMS) stars accrete a substantial portion of their final mass via material transported through circumstellar disks. However, the prediction that accretion of high angular momentum disk material will cause the stars to spin up during the accretion phase (*e.g.* Durisen et al. 1989) is not borne out by observations: most PMS stars have rotational velocities (v) of no more than a few tens of km s^{-1} . By contrast, the typical breakup velocity at ~ 1 Myr is $\sim 300 \text{ km s}^{-1}$.

Explanations of the observed slow rotation typically invoke angular momentum transfer either from the star to the surrounding accretion disk (*e.g.* Königl 1991), or to a stellar wind originating at the boundary between the disk and the stellar magnetosphere (*e.g.* Shu et al. 2000). Either mechanism requires that during the disk accretion phase, the angular velocity of the star be “locked” to a period set by the Keplerian angular velocity at or near the boundary between the stellar magnetosphere and the accretion disk. At the end of the accretion phase, PMS stars should be unlocked from their disks, and free to spin up as they contract toward the main sequence.

Considerable observational effort has been devoted to testing the prediction that rotation periods are locked to a narrow range during the accretion phase via comparison of the distribution of stellar periods or

¹National Research Council Resident Research Associate, Jet Propulsion Laboratory, California Institute of Technology, M/S 169-506, 4800 Oak Grove Drive, Pasadena, CA 91109 (luisa.rebull@jpl.nasa.gov)

²Currently Staff Scientist at SIRTf Science Center, Caltech M/S 220-6, 1200 E. California Blvd., Pasadena, CA 91125

³NOAO, 950 N. Cherry Ave, Tucson, AZ 85726

⁴STScI, 3700 San Martin Dr, Baltimore, MD 21218

rotation rates for samples of stars surrounded by disks with those that lack disks. Early studies suggested that stars surrounded by disks tend to have significantly longer rotation periods than their diskless counterparts (*e.g.* Edwards et al. 1993, Choi & Herbst 1996); more recent results based on larger samples yield more ambiguous results (*e.g.* Rebull 2001 [R01]; Stassun et al. 1999 [SMMV]; see also Herbst et al. 2000 [HRHC], Carpenter et al. 2001 [CHS], Herbst et al. 2001 [HBJM]). HRHC and HBJM both find a bimodal distribution of periods for the higher-mass ($\gtrsim 0.25 M_{\odot}$) stars, whereas it is not bimodal for the lower mass stars. R01 looked for this dependence, but did not find it.

Over the past few years, rotation periods P or projected rotational velocities $v \sin i$ have been measured for large samples of PMS stars. These data sets are now large enough to map changes in stellar angular momentum (J) as stars of different masses evolve down their convective tracks, and to understand the role that disk locking may play in determining the angular momenta of young stars.

In this paper, we exploit these large datasets to examine the early angular momentum history of PMS stars spanning ages from ~ 0.1 Myr to ~ 3 Myr and masses ~ 0.2 to $\sim 2 M_{\odot}$, both for stars apparently surrounded by accretion disks and those that lack evidence of such disks.

We first examine two samples of low mass PMS stars for which rotation periods are derived from observations of spot-modulated light variations: stars located in fields flanking the Orion Nebula Cluster and NGC 2264. Together, stars comprising these samples span masses from ~ 0.2 – $2 M_{\odot}$ and nominal ages from ~ 0.1 – 3 Myr. At fixed T_{eff} , radii appear to span a range of about a factor of 3. Absent any external angular momentum loss mechanism (*e.g.*, disk locking or spindown torques exerted by stellar winds), contraction of these fully convective stars over this radius range should result in a dramatic (9-fold) decrease in period. Hence, our sample appears well-suited to quantifying changes in period distributions among PMS stars arising as stars contract along convective tracks, and to assessing the possible role of mechanisms that could potentially regulate or mitigate such evolution-driven changes among low mass stars.

Our approach will be to examine the relationship between observed rotation period (P) and derived stellar radius (R) for a large sample of PMS stars – both those which appear surrounded by circumstellar accretion disks (as judged from near-IR excess emission), and those that appear to lack such disks. We thus first summarize the observational database for each sample: the derived periods as well as sample limitations, along with the photometry and spectroscopy that enable locating each star in the $L_{\text{bol}}-T_{\text{eff}}$ plane (thus yielding a radius) and determining whether or not a star is surrounded by a circumstellar accretion disk. Particular attention is paid to evaluating the uncertainties in derived radii – a critical factor in assessing the changes in stellar periods expected as PMS stars contract, absent external regulation.

We find that PMS stars spanning an age range from ~ 0.1 to 3 Myr do not appear to conserve stellar angular momentum as they evolve down their convective tracks, but instead preserve the same range of periods even though they have contracted by nearly a factor of three. Our conclusions apply both to stars which appear to lack the near-infrared excesses diagnostic of circumstellar accretion disks and those that show conclusive evidence of disks.

Independent supporting evidence for this result follows both from analysis of the relationship between observed periods and derived stellar radii using other recently published surveys, and from recently published projected rotational velocities observed for a sample of stars drawn from the Orion Nebula Cluster itself (Rhode et al. 2001; RHM). These latter data reveal a *decrease* of average $v \sin i$ with decreasing radius, consistent with the results derived from the ONC Flanking Fields and NGC 2264 period studies.

Together, these results seem to require a mechanism that constrains young stars to a constant range

of periods from the time they first appear on the stellar birthline to ages at least as great as ~ 3 Myr. We discuss several candidate mechanisms, the most plausible of which appears to be disk-locking.

2. Observations

This paper makes use of data sets for three young clusters: the Orion Nebula Cluster (ONC), the Flanking Fields (FF) that surround the ONC (cf. Rebull 2001), and NGC 2264. Together, these clusters allow us to examine changes in stellar angular momenta for stars with and without IR signatures of disks having ages, masses, and radii spanning the ranges $\sim 0.1\text{--}3$ Myr, $\sim 0.2\text{--}2 M_\odot$, and $\sim 1\text{--}5 R_\odot$ respectively. In order to place stars in observed and reddening-corrected color-magnitude (CMD) or Hertzsprung-Russell (HRD) diagrams, determine stellar radii, and assess whether or not a star has a disk, we require that spectral types along with VI_CK_s photometry be available for all the stars included in the present study.

We use L_{bol} and T_{eff} to calculate stellar R :

$$R^2 = \frac{L_{\text{bol}}}{4\pi\sigma T_{\text{eff}}^4} \quad (1)$$

To obtain L_{bol} and T_{eff} from the observed I_C and $V - I_C$, we first deredden the observed $V - I_C$ using the observed spectral type to estimate intrinsic colors. The dereddened I_{C0} is calculated from the extinction at I_C , which is given by $A_I = 1.61E(V - I_C)$. T_{eff} follows from the spectral type. We convert I_{C0} to L_{bol} using the approach described by Hillenbrand (1997; H97); distance moduli were taken from the literature as noted in the sections that follow.

To ensure internal consistency, we recalculated previously published extinction and color excesses for each star included in our discussion by combining photometry and spectra reported in the literature with a common set of assumed photospheric colors and reddening laws.

2.1. The ONC

The ONC is nearby (470 pc; Genzel et al. 1981), compact (size ~ 1 pc), and young (typical stellar ages of $\sim 1\text{--}3$ Myr; see, e.g. H97). It has been studied recently by Rhode et al. (2001; RHM), who measured values of the projected rotational velocity ($v \sin i$) for 155 stars (with upper limits for another 83). Observed V , I_C , and K_s colors and spectral types for these stars are available from H97. There are 202 stars for which both the photometry and measurements of $v \sin i$ are available; they appear in Figures 1–3. These figures show the observed and dereddened CMDs for the stars along with their positions in the $L_{\text{bol}}\text{--}T_{\text{eff}}$ plane (Hertzsprung-Russell Diagram, HRD). About 60% of the stars in the $v \sin i$ sample have near-infrared ($I_C - K_s$) excesses indicative of a circumstellar disk, e.g. a de-reddened $I_C - K_s$ color exceeding expected photospheric values by 0.3 mag, the conservative criterion adopted by H97 (see also Hillenbrand et al. 1998) to select the most probable disk candidates.

A significant advantage of using $v \sin i$ data for studies of PMS rotational properties is that line widths can be measured for *every* PMS star to a limit set by spectral resolution; for the RHM data this limit is 11 km s^{-1} , which corresponds to $P > 6$ days for a typical PMS star. By contrast, searches for spot-modulated periods have biases arising from: (1) the sampling cadence of photometric observations (which can be determined if the observation times are known); (2) the greater difficulty in determining periods for accreting PMS stars in which stochastic, accretion-driven photometric variability can overwhelm periodic

spot-modulated signals; and (3) the possibility that some ranges in stellar rotation rate may not produce the large, long-lived spots required to establish periodicity. Together, these biases could well mitigate the significant advantage in principle of periods in establishing stellar rotation absent the complication of projection effects ($\sin i$).

RHM establish a result essential to studies of stellar angular momenta based on observations of spot-modulated periods: there is no statistically significant difference between the $v \sin i$ distributions of PMS stars with known periods (P) and those without. Hence there is *no statistical bias introduced by determining the distribution of rotational properties for that subset of PMS for which period determinations are possible*.

RHM calculate $R \sin i$ values by combining observed P and $v \sin i$. They also establish another result critical to our analysis: agreement in the mean between these $R \sin i$ values and the R values calculated from L_{bol} and T_{eff} . This result supports our use of estimates of R derived from the apparent location of an individual star in the HRD as an independent variable that can be used to estimate the effects of evolution-driven changes in angular momentum.

2.2. The Flanking Fields

The Orion Flanking Fields (FF) were defined and studied by Rebull et al. (2000) and Rebull (2001; R01); we use $VI_C K_s$ photometry, spectral types, and P from these papers, producing 197 stars which appear in Figures 1–3.

Measures of stellar rotation for this sample are provided by spot-modulated photometric periods (P). Spot modulation is only found in late-type stars, so unlike $v \sin i$ measurements, which can be made of any type star, P observations are only obtainable for types mid-G and later. Period determinations have uncertainties $\delta P < 1\%$. The P measurements used here are complete over a broad range of periods, viz $P \sim 25 - 0.3\text{d}$, corresponding to rotational velocities $v \sim 3 - 300 \text{ km s}^{-1}$, ranging from $\sim 1-100\%$ of the breakup velocity.

We have limited our primary set of P data in Orion to the studies of the FF cited above in order to ensure that we were working with a homogenous data set that was complete over the largest possible range of periods. There are several other studies of the Orion region in the literature; they are compared in Table 1. Note that the ranges of periods over which these studies are *complete* (not simply *sensitive*) can vary widely. Results from the other databases spanning more restricted or different ranges of period nevertheless support the conclusions reached from analysis of our primary database (R01), as will be shown below.

Stars with observed periods in the FF are young and thought to be associated with the ONC cluster for several reasons. R01 used existing membership studies to demonstrate that the possible field star contamination in the sample of stars showing periodic variability is low, hence supporting the assumption that stars in the FF with derived periods are likely to be associated with the ONC. Further arguments that reinforce this contention include that: (1) the CMD of stars in these fields strongly resembles those from the ONC (see Rebull et al. 2000 and Figures 1–3), and (2) the spatial distribution of the periodic candidates is elongated N-S, along the direction defined by the distribution of dense molecular material which lies behind both the ONC and the FF. We thus adopt the same distance, 470 pc, for the FF stars as we did for the ONC sample.

R01 examines the $I_C - K_s$ excesses for the FF sample as part of her study of disk frequency and properties. She finds that 30% of the stars in the FF sample have $I_C - K_s$ excesses of 0.3 mag (or greater) above expected photospheric values – the conservative criterion adopted by H97 and Hillenbrand et al. (1998)

as indicative of stars with high likelihood of a circumstellar accretion disk.

2.3. NGC 2264

Data for NGC 2264 are similar to those used for the FF sample. Colors and spectral types come from Rebull et al. (2002), and periods from Makidon et al. (2002). A total of 81 stars have spectral types, colors, and spot-modulated periods. These stars, appearing in Figures 1–3, come from our study of NGC 2264 alone; the stars that we have in common with Kearns & Herbst (1997, 1998) are retrieved with identical periods. About 20% of the stars in this sample have $I_C - K_s$ excesses indicative of a circumstellar disk using H97’s conservative criterion, $I_C - K_s$ excess > 0.3 mag.

NGC 2264 (part of the Mon OB 1 association) is about twice as far away as Orion; we used a distance modulus of 9.40, or 760 pc (Sung et al. 1997). As in Orion, a molecular cloud located behind the cluster aids in blocking background field stars and limiting the cluster depth to a small fraction of the distance to the cluster. Past studies have argued that NGC 2264 is slightly older than the ONC at 3–5 Myr (*e.g.* Sung et al. 1997). Our data suggest that NGC 2264 indeed appears to contain fewer very young stars when compared with the ONC, but Figure 2 also suggests that the *range* of ages found in NGC 2264 is not dramatically different from the ONC (Rebull et al. 2002). The value of the NGC 2264 sample for this study thus lies in its containing a larger *fraction* of stars with ages comparable to 3 Myr than either the ONC or FF.

3. Sources of error in R

Key to our study is the ability to estimate stellar R accurately enough to track the changes in P expected as PMS stars contract and evolve down their convective tracks. The procedure for calculating R is described in the previous section. Sources of error in this calculation include photometric uncertainty, the amplitude of stellar variability, uncertainties in the reddening correction, errors in classification, uncertainties in the intrinsic photospheric colors, the effects of accretion, errors in the distance, and the presence of companions. All of these effects contribute to errors in L_{bol} and T_{eff} and hence to uncertainty in R . In the remainder of this section, we provide a thorough discussion of uncertainties involved in deriving L_{bol} , T_{eff} , and R from the observed colors and spectral types. Photometric and spectral type errors are summarized in Table 2. Unless otherwise specified, L_{bol} is in $\text{ergs cm}^{-2} \text{ s}^{-1}$, T_{eff} in K, and R in R_{\odot} .

3.1. Preliminaries

Since

$$2 \log R = \log L_{\text{bol}} - \log(4\pi\sigma) - 4 \log T_{\text{eff}} \quad (2)$$

and for

$$x = au \pm bv \quad (3)$$

the propagation of errors is described by (Bevington & Robinson 1992)

$$\sigma_x^2 = a^2 \sigma_u^2 + b^2 \sigma_v^2 \pm ab \sigma_{uv}^2, \quad (4)$$

it follows that:

$$(\delta \log R)^2 = \frac{1}{4} (\delta \log L_{\text{bol}})^2 + 4 (\delta \log T_{\text{eff}})^2 \quad (5)$$

where we assume that the errors are independent. This assumption gives an upper bound to the total error, since errors in spectral type produce partially offsetting errors in T_{eff} and L_{bol} .

3.2. Errors in Brightness and Color

Photometric errors result from photon counting statistics, uncertainties in atmospheric extinction corrections, and uncertainties in transforming to a standard system. These errors are smallest for the brightest stars and largest for the faintest stars, but are typically ~ 0.03 mag in both I_C and $V - I_C$ for most stars in our sample.

Photometric variability on scales ranging from millimagnitudes to magnitudes is characteristic of young stars (e.g. Herbig 1954). The light curves of the samples with periods (the FF and NGC 2264 stars) have typical amplitudes (mean-to-peak) of 0.03 mag in I_C for all but the stars with spectral types M3 and later, which have somewhat larger amplitudes. The $v \sin i$ sample was specifically selected to include aperiodic as well as periodic variables. We do not have monitoring information on these specific stars, but the distribution of variations of similar aperiodic stars in the FF and NGC 2264 is strongly peaked near ~ 0.03 mag as well. We therefore take ~ 0.03 mag as the typical amplitude for all stars in our samples.

In our photometric studies of the FF and NGC 2264, we monitored in one filter, I_C , only, and thus we do not have direct information on how $V - I_C$ or V changes with these periodic modulations. Carpenter et al. (2001) monitored stars including those in 2 of the 4 FF in JHK_s . They find that most (between 57 and 77%) of their variable stars can be accounted for by cool spot models, e.g. low-amplitude, nearly colorless modulations. Based on this, we assume that the amplitude of variation we found at I_C also occurs in V , and that it does not affect $V - I_C$ at significant levels.

If we assume that $V - I_C$ is affected only by uncertainties resulting from photometric uncertainties, for stars with types between K5 and M2, we derive uncertainties in luminosity $\delta \log L_{\text{bol}} \sim 0.04$; similarly $\delta \log T_{\text{eff}} \sim 0.002$. Using equation 5 above, $\delta \log R \sim 0.02$.

If we assume that I_C is affected by photometric uncertainties and by variations with an amplitude of 0.03 mag, we similarly derive, for stars with types between K5 and M2, $\delta \log L_{\text{bol}} \sim 0.02$, and $\delta \log T_{\text{eff}} \sim 0$ (because changing I_C alone does not change T_{eff}), and thus $\delta \log R \sim 0.01$. These uncertainties increase with $V - I_C$ primarily because the redder stars are also fainter.

3.3. Reddening corrections, photospheric colors, and spectral type uncertainties

We use spectral types to determine the intrinsic stellar colors and hence to derive (interstellar) reddening. The dominant error in this process is the uncertainty in spectral classification. Errors in typing have been estimated (H97, Rebull et al. 2000) to be one subclass for the earlier types (F, G, K) and at half a subclass for the later types (M). For stars that are still accreting material from their disks, the effects of veiling on the observed photospheric spectrum result in classifications that are systematically too early (e.g. H97).

Another potential source of error is uncertainty in the intrinsic photospheric colors. It is standard practice to adopt ZAMS colors as the best estimate for the true photospheric colors for these young, low-gravity stars. Our array of ZAMS colors includes measurements from Bessell (1991), Leggett (1992), and Leggett et al. (1998). This issue was discussed in detail by Rebull et al. (2000), so we only summarize some

of the most important issues here. (1) Colors for types $>M4$ are the most uncertain. (2) Chromospheric activity at levels typical of PMS stars can in principle affect PMS colors, but hot active regions are not likely to significantly affect colors for passbands V and redder (cf. Rebull et al. 2000). (3) Large dark spots can also in principle affect both colors and spectral types; their effects have not yet been quantified. (4) Finally, the use of dwarf colors for these young subgiant stars may be questionable. To place an upper bound on this latter effect, we have compared colors for dwarf stars with evolved stars of luminosity class I and II. Based on this comparison, we note that PMS stars are likely to be slightly redder than dwarfs to about M1, and bluer for stars later than that. However, the size of this error is small compared to the color change effected by assuming one spectral (sub-)class uncertainty in each direction. For example, a worst-case scenario occurs at M2, where the difference between dwarf and giant $V - I_C$ is ~ 0.25 mag. By comparison, the difference between $V - I_C$ colors of M2 and M2.5 dwarfs is ~ 0.5 mag. Since the true intrinsic colors of the PMS stars are closer to dwarfs than stars of class I and II (c.f. H97), this error will be in reality even smaller.

We have estimated the total error from all of the sources considered in this subsection by shifting the observed spectral type one subclass (or half a subclass for the M stars) blue and red, and then comparing the resulting L_{bol} , T_{eff} , and R . Typical standard errors for stars in the type range K5–M2 are $\delta \log L_{\text{bol}} \sim 0.06$, $\delta \log T_{\text{eff}} \sim 0.01$, and $\delta \log R \sim 0.04$. The uncertainties in T_{eff} increase as a function of type to mid-K owing to the uncertainty in assigning spectral types and the slope of the relationship between spectral type and T_{eff} , but decrease from late K through the M-types, because the precision of our assigned spectral types improves for these late type stars. The uncertainties in L_{bol} increase monotonically as a function of type.

We note that stars in the ONC may suffer from an additional effect: a range in the ratio of total to selective extinction that apparently derives from a spatially variable mix of interstellar grain sizes in the vicinity of the Trapezium. For a typical $V - I_C$ color excess, the uncertainty driven by a change of a factor of two in the total to selective absorption ratio will vary by ~ 0.5 mag, which corresponds to an uncertainty of $\log L_{\text{bol}}$ of ~ 0.2 dex or $\log R$ of ~ 0.1 dex.

3.4. Accretion

Material passing through a circumstellar accretion disk is funneled toward the star along magnetospheric columns, and eventually strikes the photosphere at supersonic speeds, producing hot “accretion spots” via shock heating. Evidence of these accretion spots is manifest as ultraviolet emission, well in excess of photospheric values for stars having large accretion rates. In recent papers, we have exploited excess UV emission as one of several measures used to evaluate whether a young star is surrounded by an accretion disk (*e.g.* Rebull et al. 2000, Rebull et al. 2002). For stars with high accretion rates, the accretion spot emission can be so strong as to affect V and I_C colors as well. However, stars with accretion spot emission strong enough to affect V and I_C are unlikely to be detected as periodic variables owing to the dominance of large, random, accretion-driven luminosity changes, as compared with lower amplitude spot-driven variations. Quantitative evidence of the effects of accretion on period detectability follows from analysis of the sample of pre-main sequence stars in the Orion FF. Of the stars in the present sample with excesses derived directly from photometry and spectroscopy, only 30% have detectable periods; by contrast, of the stars likely to be cluster members which lack UV excesses, 50% have periods. Consequently, we do not believe that the periodic subsample considered in this paper is dominated by stars with accretion rates sufficiently high to affect V and I_C colors.

We cannot estimate the role of accretion for the ONC sample. While the majority (60%) of these stars

have disks as judged by $I_C - K_s$ excesses >0.3 mag, we have no estimate of the distribution of UV excesses among the sample, primarily because the high and variable background in this region of the nebula precludes accurate ultraviolet photometry from the ground.

In this latter context, we note the recent estimates of the effects of accretion-driven changes on PMS star colors and derived luminosities carried out by Hartmann (2001). From analysis of a large sample of PMS stars in the Taurus-Auriga region, he finds that uncertainties in derived luminosities owing to the effects of accretion are typically 0.06 dex in $\log L_{\text{bol}}$, or 0.03 dex in $\log R$.

3.5. Distance to and width of the clusters

Uncertainty in distance to the cluster can result in a *systematic* uncertainty in derived L_{bol} and R values. From the literature, the distance to Orion is 470 ± 70 pc; that uncertainty of 70 pc translates directly to a *systematic* uncertainty of 0.07 dex in $\log R$. Similarly, NGC 2264 is at 760 ± 30 pc, which translates to a *systematic* uncertainty $\delta \log R = 0.03$. Note, however, that an error in the average distance to a cluster simply introduces a systematic *shift* in L_{bol} or R for all the stars in the cluster. An uncertainty in distance does not therefore affect the *relative* values of R within the cluster, although it will affect comparisons of clusters with each other.

The depths along the line of sight of the three groups of stars studied here appear to be small compared to their distances. The apparent angular size of the ONC is (generously) 0.5 deg, corresponding to 1% of the distance to the cluster. The scatter in luminosity introduced by variations in the distance to individual stars within the ONC is thus much smaller than other sources of error; a 1% error in L_{bol} corresponds to less than 1% error in R . As argued above, in the case of the FF, the presence of the molecular cloud and the evident association with and similarity to the young stars in the central ONC all suggest that the distance and depth of the cluster in these fields cannot be significantly different from the distance and depth of the central ONC. The cluster NGC 2264 also has a molecular cloud behind it and its depth along the line of sight is again a small fraction of the distance to the cluster.

3.6. Binaries

The presence of binaries could significantly affect the measured I_C and therefore the derived L_{bol} . The worst-case scenario is two equal-mass binaries, where the measured L_{bol} would be actually twice what it should be for a single star; in this case, it would create a 0.3 dex in $\log L_{\text{bol}}$ and thus a 0.15 dex change in $\log R$. However, the stars studied here are unlikely to have companions with primary to secondary luminosity ratios less than about 5:1. For the ONC sample, RHM obtained spectra for all of their stars and would have seen double lines either directly or in the cross-correlation peaks had the primary:secondary luminosity ratios been smaller than 5:1; they found only 7 binaries in their full sample. For the Orion FF and NGC 2264, the period sample is also unlikely to be contaminated by unresolved binaries with similar companion luminosities. Analysis of such putative binaries would reveal *two* peaks in the power spectrum analysis of their light curves were the primary:secondary luminosity ratio smaller than $\sim 5:1$. Therefore we estimate that the increase in $\log L_{\text{bol}}$ as a result of unrecognized binaries is unlikely to exceed 0.10 for any of our samples, corresponding to $\delta \log R \sim 0.05$.

3.7. Final error estimates

The errors in $\log R$ estimated above for each readily quantifiable source are summarized in Table 2 for three different mass ranges. In addition, we estimate contributions from accretion (0.03 dex), anomalous reddening appropriate to the Trapezium region (0.1 dex), and binarity (0.05 dex). For a typical star in our sample (spectral type between K5 and M2), the combination of standard errors from photometry, colors, spectra and reddening amount to 0.05 dex (c.f. Table 2). Hence, a reasonable *upper limit* to the uncertainty in $\log R$ for stars in this spectral type range would be $\sqrt{0.05^2 + 0.03^2 + 0.1^2 + 0.05^2} = 0.13$.

3.8. Comparison to other error estimates

These error estimates were derived independently of those discussed in detail by Hartigan, Strom, & Strom (1994); our error estimates of $\delta \log L_{\text{bol}}$ are identical at 0.08 dex, and our uncertainties in photometry and spectral types of $\delta \log T_{\text{eff}}$ are essentially identical (0.015 vs. 0.018 dex).

Hartmann (2001) has also provided a careful assessment of the uncertainties in L_{bol} and T_{eff} for stars in Taurus. His final error estimate for $\delta \log L_{\text{bol}}$ ranged from 0.09–0.16 dex. However, as noted previously, he adopted an error of ~ 0.06 dex in $\log L_{\text{bol}}$ as typical of the uncertainties introduced by the effects of accretion on the colors of classical T Tauri studies included in his study. Furthermore, depth for the Taurus region compared to its distance is also much larger than for our clusters, adding an additional uncertainty of 0.06 dex in $\log L_{\text{bol}}$ for Hartmann’s sample. Even if we were to adopt Hartmann’s uncertainties (clearly an upper limit to that appropriate for our sample) we would find that the error in $\log R$ is less than 0.10 dex.

3.9. External constraints on errors

As noted in §2.1, RHM estimate values of stellar radius from (1) $\log L_{\text{bol}}$ and T_{eff} ($R(\text{HRD})$), and (2) from observed periods and projected rotational velocities, $v \sin i$ ($R \sin i$). From 73 stars with both measured P and $v \sin i$ values, we deduce

$$\log R \sin i = 0.93(\pm 0.2) \log R(\text{HRD}) - 0.19(\pm 0.1) \quad (6)$$

The scatter in $\log R$ for each star is ~ 0.2 dex. Approximately 0.15 dex of this scatter arises naturally from the spread in $R \sin i$ values introduced by projection effects. The remaining error source must amount to ~ 0.13 dex, a value consistent with our upper limit error estimate for stars in the Trapezium region (see section 3.7 above).

Another external check on our error estimates is provided by the analysis of Hartigan et al. (1994). These authors estimate luminosities for individual members of PMS binary systems in the Taurus-Auriga region using methodology similar to that described above. They then compare the observed ratio $L(\text{primary}) / L(\text{secondary})$ with that expected if both stars were born at the same time, and thus fall on the same (computed) isochrone. For a sample of 29 stars, two thirds have luminosity ratios within 0.25 dex of the expected value, while 90% of the sample lies within 0.4 dex. Hence, subject to the assumption that the computed isochrones are correct, this comparison suggests that *typical* standard uncertainties in $\log R$ should be 0.12 dex or less.

4. Analysis

If stars conserve (stellar) angular momentum (J) as they evolve down their convective tracks, then we would expect that $J = I\omega$ would remain constant (where I is moment of inertia and ω is angular velocity). This is equivalent to the requirement that $J = MvR$ be constant if J is conserved in the outermost observable layer of the star. Although we expect fully convective stars to rotate as solid bodies, theoretical models of PMS stars (*e.g.* Swenson et al. 1994) predict that changes in surface rotation rate as a star evolves down the convective track are the same whether the star rotates as a solid body or conserves J locally (*i.e.* J conservation in spherical shells). The reason is that along the convective track contraction is nearly homologous, and changes in I directly track changes in R^2 . For a given mass, if J is conserved, then vR is constant and $P = 2\pi R/v \propto R^2$.

In the following sections, we examine the relationships between R and P and between R and $v \sin i$ and compare these empirical relationships with the simple prediction that stellar angular momentum is conserved, as expected absent angular momentum loss.

4.1. The FF and NGC 2264

In Figures 4 and 5, we plot P vs. R for the stars in the FF and NGC 2264. The data are shown for three different spectral type groups, which has the advantage of effectively segregating the samples by mass. In this way, we can also show the data for stars with spectral types M3 and later separately, since the errors in R are largest in this type range. This dividing line is also convenient, as (using D’Antona & Mazzitelli models) it corresponds to $\sim 0.25\text{--}0.3 M_{\odot}$; this is the location of the break in the distribution of periods as found by HRHC and HBJM.

Reference to Figures 4 and 5 (see also Fig 7) shows that the change in $\log R$ is, depending on the cluster, at least 0.6 and could be as large as 0.9. Allowing for the standard error of 0.13, it is therefore reasonable to assume that there are real changes in $\log R$ of *at least* a factor of 3, a result that is consistent with the evidence for contraction obtained by RHM. Figures 4 and 5 show that for all three mass ranges in these two clusters, there is *no evidence* for the spin-up that would be expected with decreasing R and increasing age if stellar angular momentum were conserved. Rather, they suggest *evolution at constant P , or constant angular velocity*.

While Figures 4 and 5 and the fits show no change of *average* period as PMS stars contract, it is more difficult to ascertain via inspection whether the *distribution* of periods changes significantly. To search for such a change, we plot in Figure 6 two histograms depicting the frequency distribution of P for stars in the upper and lower quartiles of derived stellar R for our sample. Values of $\langle \log P \rangle$ and $\langle \log R \rangle$ for the upper and lower quartiles are presented in Table 3; note that the average $\log R$ for the upper and lower quartiles are 0.47 ± 0.01 and 0.13 ± 0.01 respectively, whereas the average $\log P$ is 0.50 ± 0.06 and 0.58 ± 0.05 . Were all stars free to spin up in response to contraction, we would expect the shape of these histograms to be the same, but the peak among the lower quartile stars to shift to $\log P = 0.50 - 0.68 = -0.18$.

If some of the stars were ‘locked’ to fixed periods, for example by disks, while others were free to spin up, we would expect the latter objects to populate an extended ‘tail’ towards short periods in the solid lines in Figure 6. Both visual inspection and quantitative comparison of these distributions via a K-S test reveal no evidence that there is a significant difference. The fraction of stars with periods in the lowest (shortest period) quartile of the distributions in Figure 6a is 13/52 (25%) for the lower quartile in radius and 19/53

(35%) for the upper quartile. Within Poisson statistics, these fractions are identical.

We conclude from Figure 6 and the above analysis that there is no significant difference in the frequency distribution of periods among samples of stars with average $\log R \sim 0.47$ and 0.13 dex (the upper and lower quartile in radius). Hence, there is no evidence of spinup among the bulk of our sample.

The errors in P are negligible, and so the only way to invalidate this result is to hypothesize that the errors in R are much larger than we have estimated—so large, in fact, that we cannot use R to sort stars by age. If there were a wide mixture of ages at each R value, then the spin-up expected for conservation of angular momentum in diskless stars would be masked by observational scatter.

Our conclusion that there is no apparent increase in P as stars contract finds additional support from analysis of other datasets sensitive to more limited ranges of P and/or R .

Periods for stars in the ONC can be found in HRHC, SMMV, R01, CHS, and HBJM. We can perform a similar analysis of all of these data together for stars just in the ONC, defined for purposes here as the region studied by H97. Figure 7 is similar to Figures 4 and 5 but for all 292 stars with available periods, V , I_C , and spectral types. Figure 6 presents a similar analysis of the distribution of $\log P$ for the upper and lower quartiles of $\log R$ for this ONC sample; $\langle \log P \rangle$ and $\langle \log R \rangle$ are noted in Table 3. The fraction of stars with periods in the lowest (shortest period) quartile of the distributions in Figure 6a is 21/73 (29%) for the lower quartile in radius and 18/73 (25%) for the upper quartile. Within Poisson statistics, these fractions are identical to each other and to the results obtained with the FF data.

We next explore whether these results differ among samples which appear to be surrounded by disks and those which appear to lack disks. To enable as robust a comparison as possible, we consider stars from the FF sample surrounded by accretion disks to meet the conservative criterion $I_C - K_s$ excess > 0.3 mag established by H97; those which lack disks are assumed to have $I_C - K_s$ excess < 0.1 mag. We exclude stars with $0.1 < I_C - K_s$ excess < 0.3 mag from the sample on the grounds that establishing the presence or absence of a disk is less certain in these cases. Figure 8 is similar to Figure 6 but for stars with $I_C - K_s$ excesses > 0.3 and < 0.1 mag. As before, Table 3 summarizes $\langle \log P \rangle$ and $\langle \log R \rangle$. We conclude that there is no significant difference in the distribution of periods among young stars which appear very likely to be surrounded by disks and those that lack disks *based on $I_C - K_s$ excesses alone*. This result holds for both young stars with large radii and their presumed descendents which have contracted by a factor of three.

We can fit lines to the $\log P$ vs. $\log R$ relationships depicted in Figures 4 and 5 (and 7) and to a wide variety of subsets thereof. Within the scatter, fits to all of the subsets return a value consistent with zero slope. To obtain the largest range of R possible, we combined all of the data from all of the clusters and all of the surveys. (The disadvantage to doing this, in addition to the surveys' different sensitivities and completeness, is that Orion and NGC 2264 are at different distances, and if there are errors in the distance, they may affect the comparison.) We broke the entire data set into two samples, with $I_C - K_s$ excesses > 0.3 and < 0.1 . The slope of a fit to these data is 0.2 ± 0.2 for the subsample with no excesses and -0.1 ± 0.2 for the subsample with excesses. These results are consistent with a slope of zero (no change of P with R), and clearly inconsistent with the slope of 2 expected were stellar angular momentum conserved as stars contract.

4.2. The ONC

If stars indeed evolve at constant P to ages $t \sim 3$ Myr as Figures 4 and 5 suggest, then v/R should be constant. In other words, a solid prediction based on the observations of rotation periods in NGC 2264 and

the FF is that older stars with smaller radii should be rotating more slowly than younger stars with larger radii. If, on the other hand, angular momentum (J) is conserved during evolution, then vR is constant. The typical change in R over the populated portion of the convective tracks is about a factor of 3 (cf. Figures 4 and 5). If we take a typical value of v to be about 35 km s^{-1} for the youngest stars (see results of RHM below), then if J is conserved, the oldest stars should be rotating at more than 100 km s^{-1} . If angular velocity is conserved, then the oldest stars should be rotating at about 12 km s^{-1} .

We can make use of the RHM dataset to search for evolution-driven trends in rotational velocity. To do this, we have followed RHM and sorted the stars by L_{bol} and T_{eff} . Within each $(T_{\text{eff}}, L_{\text{bol}})$ ‘box’, we average the values of $v \sin i$. This approach is necessary because there is substantial scatter in the relationship between $v \sin i$ and R among the stars in this sample arising from (1) the wide range in rotational velocity at fixed R (examination of the range of observed periods at fixed radius suggests an expected range of a factor of 10), and (2) the range of inclination ($\sin i$) values.

In Figure 9, we superpose the $(T_{\text{eff}}, L_{\text{bol}})$ ‘boxes’ on an HR diagram. Also plotted are the stars observed by RHM and a set of evolutionary tracks. This diagram shows that the stars observed in the Rhode et al. ONC survey span the mass range $\sim 0.2\text{--}2.0 M_{\odot}$. Note also that stars evolve down convective tracks at nearly constant T_{eff} . The RHM approach of sorting the stars by L_{bol} and T_{eff} also approximately sorts them by age and mass. Each vertical column in the grid shown in Figure 9 spans a range of masses of about 30% around the mean mass. The convective tracks are not exactly vertical in this diagram, and so some stars of a given mass may move from one column to the next adjacent one as they evolve down their tracks. However, given that $\langle v \sin i \rangle$ at a given luminosity shows no systematic trend with $\log T_{\text{eff}}$ (see Figure 10), then the small change in average mass with decreasing L_{bol} within a T_{eff} column will not bias the results significantly.

As discussed above, the errors in $\log L_{\text{bol}}$ and $\log T_{\text{eff}}$ are estimated to be 0.08 and 0.015 respectively. The width of the bins into which the stars were placed are 0.37 in $\log L_{\text{bol}}$ and 0.048 in $\log T_{\text{eff}}$. It is therefore unlikely that the errors in deriving $\log L_{\text{bol}}$ and $\log T_{\text{eff}}$ are large enough to move a star further than to a bin just adjacent to its true location. In most of the mass ranges studied, the stars span nearly 1.5 in $\log L_{\text{bol}}$, and so the errors in $\log L_{\text{bol}}$ are not large enough to mask systematic trends in $\langle v \sin i \rangle$ as a function of L_{bol} . Because (cf. Figure 10) there are no systematic trends in $v \sin i$ with T_{eff} at constant L_{bol} , errors in T_{eff} are not large enough to introduce or mask any systematic trends.

Figure 10 shows this same rectangular grid, but now with lines of constant radius superposed. Comparing this figure with Figure 9 shows that the data for stars in a given mass range typically span a factor of ~ 3 in radius. The average value of $v \sin i$ for the stars within each of the grid boxes is also shown. The data are summarized in Table 4, which gives $\langle v \sin i \rangle$, its standard deviation, and the number of stars in each grid box.

Examination of Figure 10 shows that stars near the tops of the convective tracks have $v \sin i$ typically about 35 km s^{-1} . Stars near the bottom of the tracks have typical $v \sin i$ of about 20 km s^{-1} —*far smaller than the 105 km s^{-1} that would be expected for conservation of stellar angular momentum*. Instead, the observed value of 20 km s^{-1} is about 50% higher than the 12 km s^{-1} that would be expected for conservation of angular velocity. However, these results are biased toward minimizing the decrease in $v \sin i$ with R . In calculating these averages, we have used 11 km s^{-1} for all stars rotating at or below the resolution limit set by the spectra analyzed by RHM. Typically 20% or fewer of the stars at the tops of the convective tracks are rotating at or below this limit, and so $\langle v \sin i \rangle$ for the youngest stars should not be significantly overestimated because of the inclusion of stars with measured upper limits. However, *more than half* of the stars at the bottoms of the tracks rotate at or below 11 km s^{-1} , and so the values of $\langle v \sin i \rangle$ quoted for the

oldest stars are too high. This increase in the fraction of stars with $v \sin i < 11 \text{ km s}^{-1}$ is another indicator that stellar angular momentum is lost as stars evolve down their convective tracks.

Note, too, that the decrease in $\langle v \sin i \rangle$ with decreasing radius and increasing age is found independently for each of the columns in Figure 10.

We can estimate the significance of this result by plotting the values of $\langle v \sin i \rangle$ for each of the $(T_{\text{eff}}, L_{\text{bol}})$ boxes against the average value $\langle R \rangle$ for each box; this relationship is shown in Figure 11. Note (c.f. Fig. 10) that $\langle v \sin i \rangle$ is nearly constant along lines of constant R , and we can therefore combine the data for stars of all masses spanned by the RHM sample. From Fig. 11, we derive a formal relationship

$$\log \langle v \sin i \rangle = 0.49(\pm 0.11) \log \langle R \rangle + 1.15(\pm 0.05) \quad (7)$$

assuming uncertainties of 25% in $\langle v \sin i \rangle$ and in $\log \langle R \rangle$. Upper limits are set to 11 km s^{-1} in computing $\langle v \sin i \rangle$ for each box.

The positive slope clearly shows that the rotation of stars in this sample *slows down* as stellar radii *decrease*. The slope of the relation is clearly inconsistent with the slope of -1 that would be expected were stars conserving angular momentum as they evolve.

Table 5 gives for each grid box the product $\langle v \sin i \rangle R$, which should remain constant down each column if angular momentum is conserved, and $\langle v \sin i \rangle / R$, which should remain constant if angular velocity is conserved. Within a factor of 2 or better (especially given the 11 km s^{-1} upper limit on $v \sin i$), angular velocity is conserved for this ensemble of stars. If we calculate rotational velocities for the FF and 2264 samples using the derived values of R and observed P , we find the same trend toward decreasing rotation with decreasing R as in the ONC.

Since 60% of the ONC stars appear to have disks (based on having observed $I_C - K_s$ excesses $> 0.3 \text{ mag}$), one might conclude on the basis of this sample alone that we have found strong evidence for disk-locking – the most plausible explanation for the apparent decrease in stellar angular momentum with decreasing radius/increasing age. As we have seen, however, when we looked at the period data for the FF and NGC 2264, we found similar evidence for loss of stellar angular momentum in samples of PMS stars that appear to be dominated by objects that lack detectable disks using the same detection criteria.

4.3. Summary of the Observations

PMS stars appear to preserve the same distribution of periods over radii spanning $1\text{--}5 R_{\odot}$, corresponding to ages 0.1–3 Myr. The fact that several different mass groupings of stars in all three clusters show this same result, combined with the fact that the independent data sets for the each cluster are characterized by different sources of error, appear to make this a robust conclusion.

If correct, our results require that PMS stars lose angular momentum over this age and radius range. We explore several candidate mechanisms below.

5. Discussion

5.1. Disk Locking

Disk locking provides the most plausible explanation for the above results. However, as noted above, we find that the bulk of our sample lack robust evidence of disks, at least as measured by Hillenbrand’s conservative criterion, $I_C - K_s$ excess > 0.3 mag. Smaller values of $I_C - K_s$ excess are expected if (1) the optically thick accretion disks that produce $I_C - K_s$ excesses are viewed nearly equator on; or (2) these disks have large inner holes resulting from interruption of the accretion disk by the stellar magnetosphere at radii exceeding $5 R_*$ – a possible outcome if the stellar magnetic field is much larger than the few kilogauss typical of TTS or if the disk accretion rate is much smaller than the value of 10^{-8} typical of young TTS. In the former case, the radiating area of the disk projected in the observer’s direction is small, thus resulting in small near-IR excesses, while in the latter case, the inner disk lacks dust heated to temperatures sufficient to produce a $I_C - K_s$ excess. Moreover, observational errors in estimating the $I_C - K_s$ excess could result in missing a significant fraction of stars with relatively small excesses.

To explore the possibility that our sample might contain a significant fraction of disks with small near-IR excesses, we recalculated the fraction of disks for N2264, the ONC and the FF adopting as a criterion $I_C - K_s$ excess > 0.1 mag. The computed fractions increased from 18, 35, and 58% for $I_C - K_s$ excess > 0.3 to 59, 71, and 78%. This suggests that it is at least *plausible* that a much larger fraction of our sample could be surrounded by disks, and hence that disk locking might well account for the apparent decrease in stellar angular momenta as PMS stars contract.

Support for this speculation is also found from the recent study by Lada et al. (2000). These authors undertook an L -band search for disks, noting (1) the much larger excesses above photospheric levels expected at L ; and (2) the relative insensitivity of L to the presence of small inner disk holes. They found that about 45 percent of the M-type stars in the Trapezium had K -band excesses as judged from their location in the $J - H/H - K$ diagram but that about 80 percent of them had excesses at L .

A second search for disks with large inner holes was conducted by Stassun et al. (2001), who searched for $10 \mu\text{m}$ excesses in stars in Taurus-Auriga and Orion that lack $I_C - K_s$ excesses. In this case, only 3 of 32 stars showed evidence of $10 \mu\text{m}$ excesses, and on this basis the authors argue that most of the stars without near-IR excesses do indeed lack disks.

From these two studies, it is therefore difficult to estimate what fraction of stars surrounded by disks are missed using $I_C - K_s$ excess as a disk discriminant.

Thus, while it appears tempting to argue that disk-locking accounts for the apparent immutability of the period distribution among contracting PMS stars, more work is needed in order to establish samples of PMS stars for which periods are available and for which there is *definitive* evidence establishing the presence or absence of accretion disks.

SIRTF observations promise the sensitivity for rapid and accurate $3\text{--}10 \mu\text{m}$ surveys capable of identifying disk candidates unambiguously. SIRTF should also establish the (unlikely but still plausible) existence of gaseous accretion disks in which all but a fraction of an Earth mass of the small dust grains responsible for producing excess IR emission have been agglomerated into larger bodies.

5.2. Disk-Locking Combined with Birthline Effects

Could the combination of similar period distribution for stars of apparently different ages/radii and the lack of clear distinction in the period distribution among stars with and without disks be explained through some other mechanism?

As one possibility, suppose that (1) stars in Orion and NGC 2264 were born in a single burst of star formation ~ 1 Myr ago; (2) the range in L (equivalently R) for the PMS stars in these clusters does not reflect evolution down convective tracks, but rather differences in mass accretion rate (\dot{M}) that force stars to evolve along different ‘birthlines’ and therefore to arrive at different initial luminosities along the convective tracks (Palla & Stahler 1992); and (3) PMS stars are locked to a particular P so long as they are surrounded by accretion disks. In this picture, the observed distribution of stars along a convective track for a given mass then reflects a range of \dot{M} : protostars with higher \dot{M} have larger initial radii and lie higher in the color-magnitude diagram following the end of the accretion phase (see also Hartmann et al. 1997). The similarity of P at different R then follows from the assumption that stars are locked to their disks for much (nearly all) of their ~ 1 Myr accretion phase.

The main difficulty with this proposal lies with the additional requirement that stellar L cannot have decreased much since the stars were deposited on their convective tracks. If stars that formed through high \dot{M} and were initially deposited high on their convective tracks had subsequently evolved downwards, we would expect to see a ‘tail’ of stars that have spun up to shorter P mixed in with the ensemble of objects that started their evolution at smaller R . We do not (see Figure 6). The only way to resolve this contradiction and still maintain conservation of stellar J would be to identify a mechanism for halting or slowing evolution of stars deposited high on their convective tracks for a time comparable to at least ~ 3 Myr.

5.3. Angular Momentum Loss via Stellar Winds

Stellar winds loaded onto open magnetic field lines can exert a spindown torque on stars. However, this mechanism appears to be ineffective for PMS stars because, during this phase of evolution, the timescale for spindown exceeds the evolutionary timescale by a few orders of magnitude (*e.g.* MacGregor and Charbonneau 1994) – fully convective stars are assumed to rotate as solid bodies, and the wind must slow down the entire star.

Calculations (*e.g.* Kawaler 1988) show that the rate of change of J depends on the product of the mass loss rate and the square of the Alfvén radius, but the Alfvén radius varies inversely as some power of the mass loss rate, with the specific power depending on the configuration of the magnetic field. For a field geometry “intermediate” between a dipolar and a radial field, dJ/dt does not depend on mass loss rate at all (Bouvier et al. 1997). The only circumstance under which magnetic winds could play an important role in slowing the rotation of PMS stars would be if there were some way in which to decouple the outer layers of the star from the interior, *i.e.* if J were conserved locally, and the wind had to slow down only a thin outer layer of the star. Such decoupling is not expected for fully convective stars.

A further challenge to any wind-driven J loss mechanism is the additional requirement that significant J loss would have to cease on timescales of no more than a few Myr in order to account for the significant population of stars that ultimately arrive on the main sequence as the rapid rotators observed in young clusters such as α Persei (*e.g.* Stauffer et al. 1989); such stars require spinup from the PMS to the ZAMS.

5.4. Angular Momentum Loss via Tidally-Locked Planetary Companions

Recent theoretical models indicate that tidal locking between a close-in Jupiter-mass planet and the parent star can transfer spin J from the star to the orbital J of the planet, thus slowing the rotation of the star while driving the planet into a larger orbit.

This effect is not large enough to account for the observations reported here. The difficulty lies in the apparent incompatibility of two requirements: (1) the putative planet must be located close enough to the star to produce significant tidal distortion; and (2) the planet must be located far enough from the star to dominate the J of the system (and thus be able to create significant changes in stellar J with only modest orbital evolution). A simple calculation (cf. Trilling et al. 1998) in which we assume a Jupiter-mass planet orbiting a PMS star at a distance of 0.1 AU suggests that J regulation by tidal locking to such a planet fails by 2 orders of magnitude.

6. Summary

The observations of PMS stars discussed here span an age range of about 3 Myr and a change in stellar radius of about a factor of 3. Surprisingly, observations of both rotation periods and projected rotational velocities for a sample of several hundred stars show that most of the stars, whether surrounded by observable disks or not, preserve constant angular velocity ω to within a factor of 2 as they evolve downward along their convective tracks – and thus must lose stellar angular momentum J in direct proportion to R^2 .

A recent theoretical paper by Tinker, Pinsonneault, & Terndrup (2002) also concluded that stars must lose significant amounts of angular momentum during the first few million years after they arrive at the birthline. These authors assumed that the ONC stars, when they reach an age of 120 Myr, should produce a rotational velocity distribution that looks like the distribution in the Pleiades, and then calculated how the angular momentum of the ONC stars would have to change with time to achieve this outcome. Tinker et al. concluded that there must be a mechanism in addition to stellar winds that produces loss of stellar angular momentum. They further showed that, if this mechanism is disk-locking, then it must be effective for *all* stars up to an age of about 3 Myr, or alternatively disks must have a *range of lifetimes* over which they serve as effective brakes, and that these lifetimes extend up to 6 Myr in some stars.

These theoretical ideas combined with recent estimates for the lifetimes of disks may explain why we have not yet detected evidence for spin up in the samples we have observed. In particular, Haisch, Lada, & Lada (2001) show that more than 80% of the stars in NGC 2024, which is about 10^6 years old have IR excesses indicative of disks, while only 50% of the stars in NGC 2264, which they estimate to have an mean age of 3×10^6 years, have such excesses. Assume that all stars with ages 10^6 years and less are surrounded by disks and that during this time, their rotation periods are locked. Suppose further that half of these stars lose their disks sometime between 10^6 and 3×10^6 years. Reference to Figures 4, 5, and 7 shows that fully half of our sample stars have ages ~ 1 Myr or less and thus are, by hypothesis, locked to their disks. The remaining stars in our sample have ages between ~ 1 and ~ 3 Myr. Of those stars, at least half should still be surrounded by disks. Hence less than a quarter of our sample might be free to spin up, and most of these objects are likely to have lost their disks within the past 1 Myr, and not have spun up significantly. If these estimates of disk lifetimes are correct, it seems plausible that for the distribution of ages represented among our sample stars and the likely distribution of disk lifetimes, that such modest spinup might well be masked by the intrinsic spread in P characteristic of the youngest (presumably disk-locked) stars in our sample.

The essential point, however, is that both the observations reported here and theory seem to require that a braking mechanism—whatever it may be—must be effective for most pre-main sequence stars during at least the first 3 Myr or so after they reach the birthline.

Significant spin-up must ultimately occur in at least some stars in order to account for the rapid rotators seen on the main sequence in young clusters such as Alpha Persei (Stauffer et al. 1989). However, recent observations of $v \sin i$ for a small sample of stars in the 10 Myr old TW Hya association (Torres et al. 2001; Sterzik et al. 1999) suggest mean $v \sin i$ values similar to those found among the oldest stars in our NGC 2264 sample, despite the fact that the nominal radii among the TW Hya stars are smaller by 50%. These observations suggest that “ ω locking” may extend to 10 Myr and makes urgent the need for a campaign focused on mapping the angular momentum evolution of low mass stars in the age range 3–30 Myr so as to understand when rotational spinup in response to contraction takes place. Additionally, it would help to have an age indicator other than radius or else to show that radius correlates at least roughly with independent age estimates for clusters other than the ONC.

We wish to thank Jonathan Lunine and Lee Hartmann for several helpful discussions regarding possible explanations for the apparent paradox explored here. We wish to thank our referee Bill Herbst for extensive comments on the original manuscript. SES acknowledges support from the NASA Origins of Solar Systems program which enabled analysis of the NGC 2264 data. We thank Mark Adams for multiple comments and support during the early phases of the investigation of periodic stars and the McDonald Observatory for the award of guest investigator time on the 0.9m telescope. The research described in this paper was partially carried out at the Jet Propulsion Laboratory, California Institute of Technology, under a contract with the National Aeronautics and Space Administration.

REFERENCES

- Barnes, S. A. 2001, *ApJ*, 561, 1095
- Bessell, M. S. 1991, *AJ*, 101, 662
- Bevington, P. R., & Robinson, D. K. 1992, *Data Reduction and Error Analysis for the Physical Sciences* (2d ed; New York: McGraw-Hill)
- Bouvier, J., Forestini, M., & Allain, S. 1997, *A&A*, 326, 1023
- Carpenter, J. M., Hillenbrand, L. A., & Skrutskie, M., F. 2001, *AJ*, 121, 3160 (CHS)
- Choi, P., & Herbst, W. 1996, *AJ*, 111, 283
- D’Antona, F., & Mazzitelli, I., 1994, *ApJS*, 90, 467
- Durisen, R. H., Yang, S., Cassen, P., & Stahler, S. 1989, *ApJ*, 345, 959
- Edwards, S., Strom, S. E., Hartigan, P., Strom, K. M., Hillenbrand, L. A., Herbst, W., Attridge, J., Meriill, K. M., Probst, R., & Gatley, I., 1993, *AJ*, 106, 372
- Genzel, R., Reid, J. J., Moran, J. M., & Downes, D. 1981, *ApJ*, 244, 884
- Haisch, K., Lada, E., & Lada, C. 2001, *ApJ*, 553, 153

- Hartigan, P., Strom, K., & Strom, S., 1994, *ApJ*, 427, 961
- Hartmann, L. 2001, *AJ*, 121, 1030
- Hartmann, L., Cassen, P., & Kenyon, S. J. 1997, *ApJ*, 475, 770
- Herbig, G. 1954, *ApJ*, 119, 483
- Herbst, W., Bailer-Jones, C. A. L., & Mundt, R. 2001, *ApJ*, 554, 197 (HBJM)
- Herbst, W., Rhode, K., Hillenbrand, L., & Curran, G. 2000, *AJ*, 119, 261 (HRHC)
- Hillenbrand, L. A. 1997, *AJ*, 113, 1733
- Hillenbrand, L. A., et al. 1998, *AJ*, 116, 1816
- Kawaler, S. D. 1988, *ApJ*, 333, 236
- Kearns, K., & Herbst, W., 1997, *AJ*, 114, 1098
- Kearns, K., & Herbst, W., 1998, *AJ*, 116, 261
- Königl, A. 1991, *ApJ*, 370, 39
- Leggett, S. K. 1992, *ApJS*, 82, 351
- Leggett, S. K., Allard, F., Hauschildt, P. H. 1998, *ApJ*, 509, 836
- Lada, C. J., et al. 2000, *AJ*, 120, 3162
- MacGregor, K. B., & Charbonneau, P. 1994, in *ASP Conf. Ser. 64, Cool Stars, Stellar Systems, and the Sun, Eighth Cambridge Workshop*, ed. J.-P. Caillaut (San Francisco:ASP), 174
- Makidon, R., Rebull, L., Strom, S., Adams, M., & Patten, B. 2002, in preparation
- Palla, F., & Stahler, S. W. 1992, *ApJ*, 392, 667
- Rebull, L. M. 2001, *AJ*, 121, 1676
- Rebull, L. M., Hillenbrand, L., Strom, S. E., Duncan, D. K., Patten, B. M., Pavlovsky, C. M., Makidon, R., & Adams, M. T. 2000, *AJ*, 119, 3026
- Rebull, L. M., Makidon, R. B., Strom, S. E., Hillenbrand, L. A., Birmingham, A., Patten, B. M., Jones, B. F., Yagi, H., & Adams, M. T. 2002, *AJ*, in press
- Rhode, K. L., Herbst, W., & Mathieu, R. D. 2001, *AJ*, 122, 3258 (RHM)
- Soderblom, D., et al. 1999, *AJ*, 118, 1301
- Shu, F., Najita, J., Shang, H., & Li, Z.-Y. 2000, in *Protostars and Planets IV*, ed. V. Mannings, A. P. Boss & S. S. Russell (Tucson: University of Arizona Press), 789
- Siess, L., Dufour, E., & Forestini, M., 2000, *A&A*, 358, 593
- Stassun, K. G., Mathieu, R. D., Mazeh, T., & Vrba, F. J. 1999, *AJ*, 117, 2941 (SMMV)
- Stassun, K. G., Mathieu, R. D., Vrba, F. J., Mazeh, T., Henden, A. 2001, *AJ*, 121, 1003

Table 1: Surveys of stars in the Orion region

description	SMMV ^a	HRHC ^a	R01 ^a	CHS ^a	HBJM ^a
# stars monitored	2279	829	3585	17,808	2294
monitoring band	I_C	I_C	I_C	JHK	I_C
# periods reported	254	134	281	233	369 ^b
range of sensitivity (d)	0.1–10	1–35? ^c	0.2–40	1–13	0.2–30? ^c
range of completeness (d)	0.1–6	1–? ^c	0.3–20	2–10	0.8–15? ^c
approx. mass range (M_\odot)	0.15–1.0	0.2–2.0	0.2–1.3	0.2–1.0	0.1–1
# stars used here ^d	142 (93)	95 (30)	220 (173)	70 (16)	211 (145)

^aSMMV=Stassun et al. (1999), HRHC=Herbst et al. (2000), R01=Rebull (2001), CHS=Carpenter et al. (2001), HBHM = Herbst et al. (2001)

^b404 stars were reported in HBJM, but 369 remain in the most current list provided by W. Herbst.

^cThe range over which this study is complete is not reported, and completeness cannot be determined without specific times of observations, which are also not reported.

^dThe most significant limitation on the databases is that we require that spectral types and VI_CK_s photometry be available for all the stars included in the present study. However, because of significant overlap in each of these Orion fields, there are of course duplicate stars in these databases. The second number in parentheses in each column denotes the number of stars actually used here from the corresponding database. For example, there are 142 stars in the SMMV database for which SMMV measured a period, but only 93 for which they alone measured a period (or have the best period available). In the remaining 49 stars, another more recent study retrieved an identical period, or has made a convincing case that it has the better period for those stars.

Stauffer, J. R., Hartmann, L. W., & Jones, B. F. 1989, ApJ, 346, 160

Sterzik, M., Alcalá, J., Covino, E., Petr, M. 1999, A&A, 346, L41

Sung, H., Bessell, M. S., & Lee, S-W. 1997, AJ, 114, 2644

Swenson, F. J., Faulkner, J., Rogers, F. J., & Iglesias, C. A. 1994, ApJ, 425, 286

Tinker, J., Pinsonneault, M., & Terndrup, D. 2002, ApJ, 564, 877

Torres, G., Neuhauser, R., & Latham, D., 2001, astro-ph/0105132, to appear in Young Stars Near Earth: Progress and Prospects, 2001, Jayawardhana, R., & Greene, T., eds.

Trilling, D. E., Benz, W., Guillot, T., Lunine, J. I., Hubbard, W. B., & Burrows, A. 1998, ApJ, 500, 428

Table 2. Mean magnitude of empirically-derived errors

category	uncertainty	<K5	K5–M2	>M2
photometric	$\delta \log T_{\text{eff}}$	0.004	0.002	0.002
in $V - I$	$\delta \log L_{\text{bol}}$	0.052	0.044	0.039
(§3.2)	$\delta \log R$	0.027	0.022	0.020
photometric	$\delta \log T_{\text{eff}}$	0	0	0
in $I +$	$\delta \log L_{\text{bol}}$	0.017	0.025	0.022
amplitude (§3.2)	$\delta \log R$	0.009	0.013	0.011
spec type	$\delta \log T_{\text{eff}}$	0.013	0.012	0.010
(§3.3)	$\delta \log L_{\text{bol}}$	0.047	0.063	0.119
	$\delta \log R$	0.035	0.040	0.063
net mean	$\delta \log T_{\text{eff}}$	0.014	0.012	0.010
	$\delta \log L_{\text{bol}}$	0.072	0.081	0.127
	$\delta \log R$	0.050	0.050	0.070
typical	$\delta \log T_{\text{eff}}$		0.01	
	$\delta \log L_{\text{bol}}$		0.08	
	$\delta \log R$		0.05	

Table 3. Mean $\log P$ and $\log R$ for upper and lower quartiles in $\log R$ (see text)

sample	upper $\langle \log P \rangle$	upper $\langle \log R \rangle$	lower $\langle \log P \rangle$	lower $\langle \log R \rangle$	KS prob ^a	χ^2 prob ^a
FF	0.50±0.06	0.47±0.01	0.58±0.05	0.13±0.01	0.22	0.74
ONC	0.61±0.04	0.54±0.01	0.57±0.04	0.15±0.01	0.54	0.63
FF disks ^b	0.47±0.09	0.53±0.02	0.62±0.09	0.16±0.03	0.07	0.20
FF no disks ^c	0.58±0.10	0.41±0.02	0.46±0.09	0.10±0.02	0.30	0.37

^aThe probability derived from a two-sided K-S test of the continuous (or χ^2 test of the binned) distributions of $\log P$ for the upper quartile of $\log R$ compared with that for the lower quartile of $\log R$. Neither the χ^2 nor the KS test suggest any statistically significant difference between the upper and lower quartiles.

^bThose stars with $I_C - K_s$ excesses > 0.3 mag

^cThose stars with $I_C - K_s$ excesses < 0.1 mag

Table 4. Distribution of $v \sin i$ for the ONC stars.

$\log T_{\text{eff}}^{\text{a} \rightarrow}$ $\log L/L_{\odot}^{\text{a} \downarrow}$	A (3.730-3.682)		B (3.682-3.634)		C (3.634-3.586)		D (3.586-3.538)		E (3.538-3.490)	
	$\langle v \sin i \rangle$	num ^b	$\langle v \sin i \rangle$	num	$\langle v \sin i \rangle$	num	$\langle v \sin i \rangle$	num	$\langle v \sin i \rangle$	num
1 (1.48 - 1.11)	33±13	3	41±10	5						
2 (1.11 - 0.74)	30±4	6	26±6	4	14	1				
3 (0.74 - 0.37)	26±5	7	15±4	4	34±12	7	35±9	5		
4 (0.37 - 0.00)	19±7	2	17±3	13	17±3	18	23±4	17	34±15	3
5 (0.00 - -0.37)	12	1			20±8	6	19±3	41	19±2	22
6 (-0.37 - -0.74)					18±7	3	16±4	18	20±3	44

^aSubdivisions defined exactly as in RHM; subdivisions according to T_{eff} and L correspond to subdivisions by M for stars on convective tracks, and with age for stars of a given M . Column A from RHM spans a larger range of masses than the other columns, which span $\log M/M_{\odot} \sim 0.1$ dex when calculated via D’Antona & Mazzitelli (1994) or Siess et al. (2000).

^bNumber of stars in the bin.

Table 5. Trends in angular momentum ($\propto vR$) and angular velocity ($\propto v/R$) for the ONC.

$\log T_{\text{eff}}^{\text{a} \rightarrow}$ $\log L/L_{\odot}^{\text{a} \downarrow}$	A (3.730-3.682)		B (3.682-3.634)		C (3.634-3.586)	
	$\langle v \sin i \rangle / R^{\text{b}}$	$\langle v \sin i \rangle \times R^{\text{b}}$	$\langle v \sin i \rangle / R$	$\langle v \sin i \rangle \times R$	$\langle v \sin i \rangle / R$	$\langle v \sin i \rangle \times R$
1 (1.48 - 1.11)	6	191	6	296		
2 (1.11 - 0.74)	8	112	6	123	2	82
3 (0.74 - 0.37)	11	64	5	46	9	131
4 (0.37 - 0.00)	12	31	8	34	7	43
5 (0.00 - -0.37)	11	13			12	33
6 (-0.37 - -0.74)					17	19

^aSubdivisions defined exactly as in RHM; subdivisions according to T_{eff} and L correspond to subdivisions by M for stars on convective tracks, and with age for stars of a given M . Column A from RHM spans a larger range of masses than the other columns, which span $\log M/M_{\odot} \sim 0.1$ dex when calculated via D’Antona & Mazzitelli (1994) or Siess et al. (2000).

^b $\langle v \sin i \rangle / R$ would be constant if stellar J is conserved, and $\langle v \sin i \rangle \times R$ would be constant if ω conserved. Note that $\langle v \sin i \rangle / R$ is within a factor of ~ 2 .

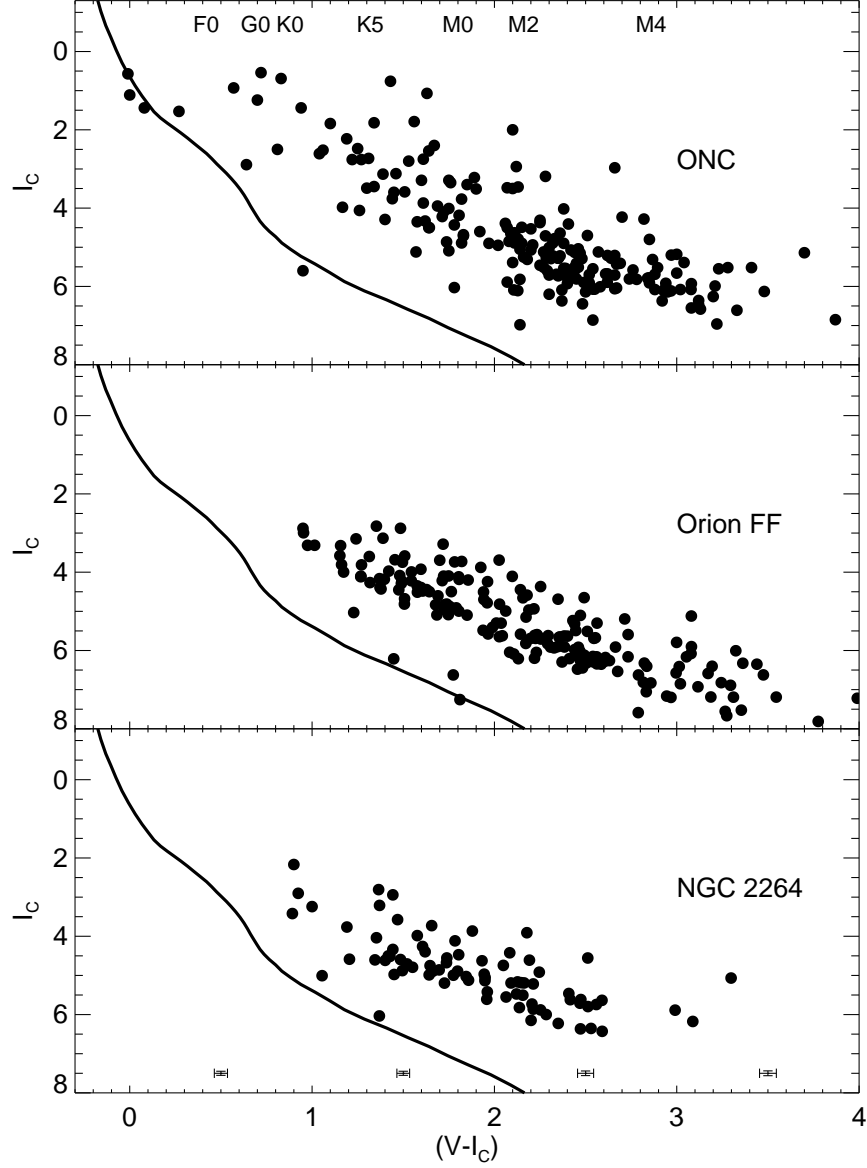


Fig. 1.— Observed color-magnitude diagram (CMD) for each of the three samples considered in this paper: the Orion Nebula Cluster itself, the Orion Nebula Cluster Flanking Fields, and NGC 2264. I_C magnitudes have been converted to absolute magnitudes (see text for adopted distance moduli) for ease of comparison between the Orion samples and NGC 2264. ZAMS relation is heavy line, and $V - I_C$ colors corresponding to various spectral types are indicated in top panel. In bottom panel, typical standard error bars are indicated for points with $V - I_C$ between 0–1, 1–2, 2–3, & 3–4; see text.

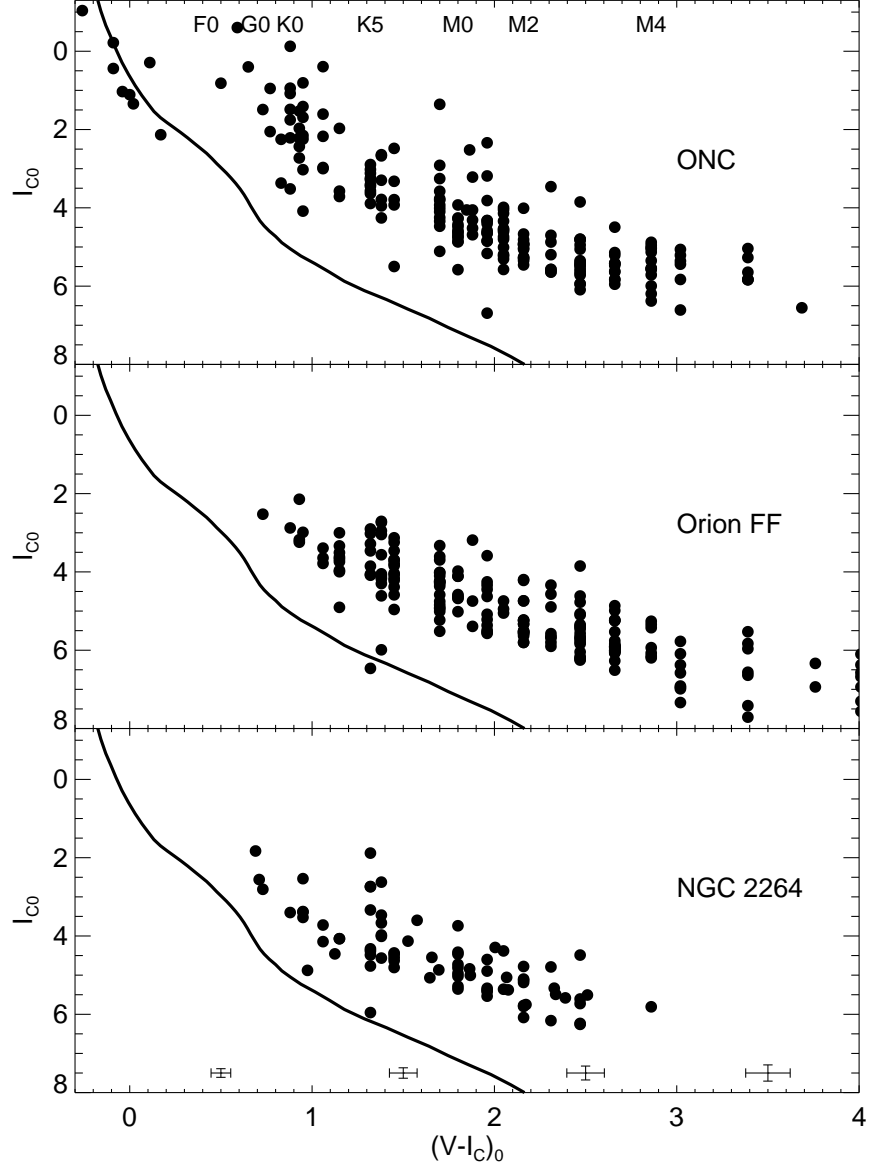


Fig. 2.— Dereddened CMD for each of the three samples considered in this paper: the Orion Nebula Cluster Flanking Fields, the Orion Nebula Cluster itself, and NGC 2264. I_C magnitudes have been corrected to absolute magnitudes for ease of comparison between the Orion samples and NGC 2264. $V - I_C$ values appear “quantized” because stars have been reddening-corrected to the intrinsic $V - I_C$ colors expected for their spectral types. ZAMS relation is heavy line, and $V - I_C$ colors of spectral types are indicated in top panel. In bottom panel, typical standard error bars are indicated for points with $V - I_C$ between 0–1, 1–2, 2–3, & 3–4; see text.

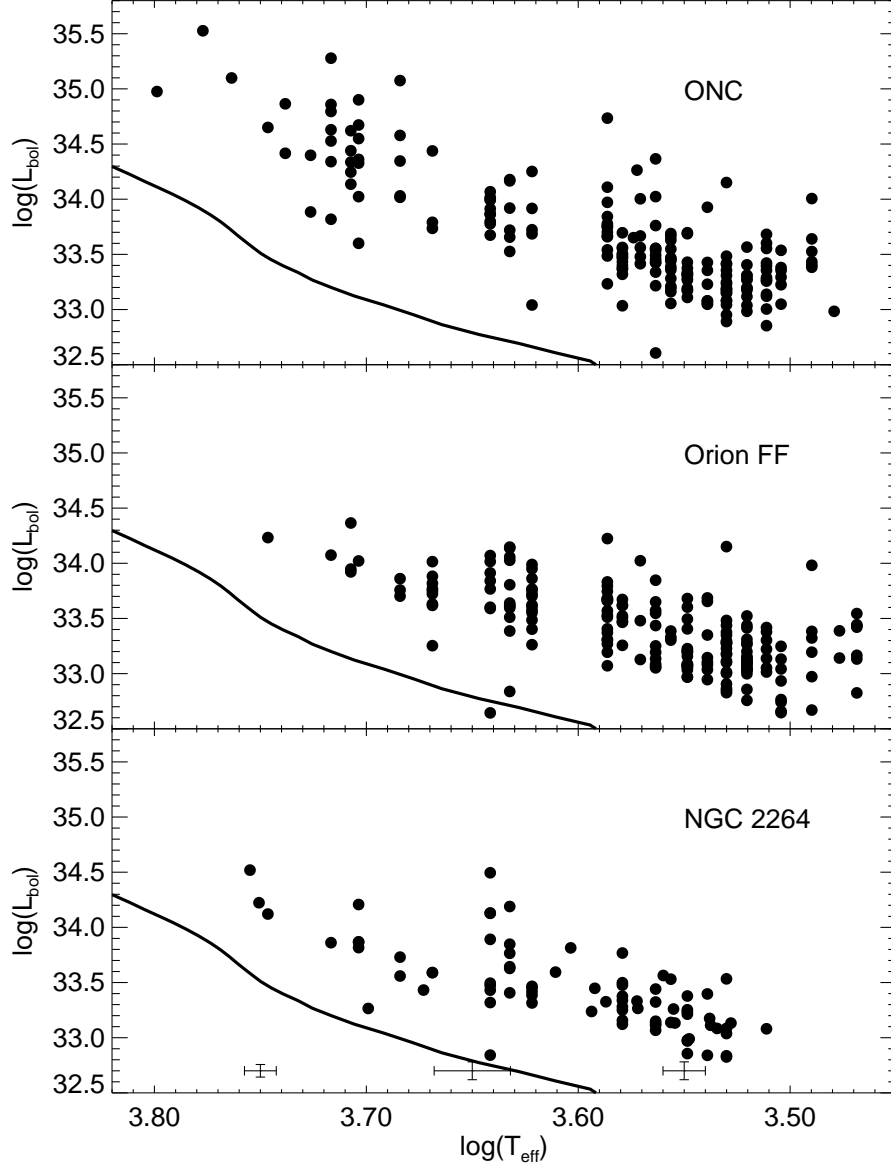


Fig. 3.— Theoretical Hertzsprung-Russell Diagrams (HRD) for each of the three samples considered in this paper: the Orion Nebula Cluster Flanking Fields, the Orion Nebula Cluster itself, and NGC 2264. L_{bol} and T_{eff} have been derived from dereddened colors following the formulas given in Hillenbrand (1997). ZAMS relation is heavy line, and $V - I_C$ colors corresponding to various spectral types are indicated on top panel. In bottom panel, typical standard error bars are indicated for points with $\log T_{\text{eff}}$ between 3.5–3.6, 3.6–3.7, & 3.7–3.8; see text.

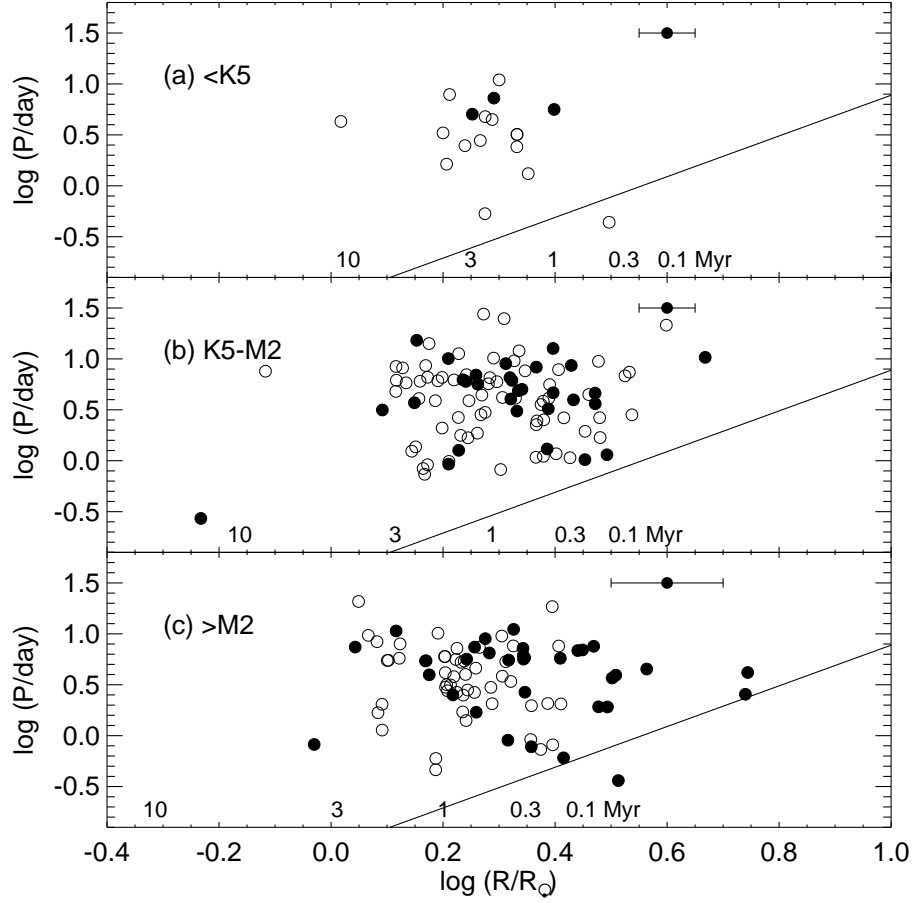


Fig. 4.— Period vs. radius for stars in the FF. (a) stars with types K5 and earlier; (b) stars with types K5-M2; (c) stars with types M3 and later. Open circles are stars without $I_C - K_s$ excesses (i.e. without disks) and solid circles are stars with excesses (i.e. with disks). Typical standard error bars for each type range are indicated. The line in each panel indicates the slope expected if stellar angular momentum is conserved.

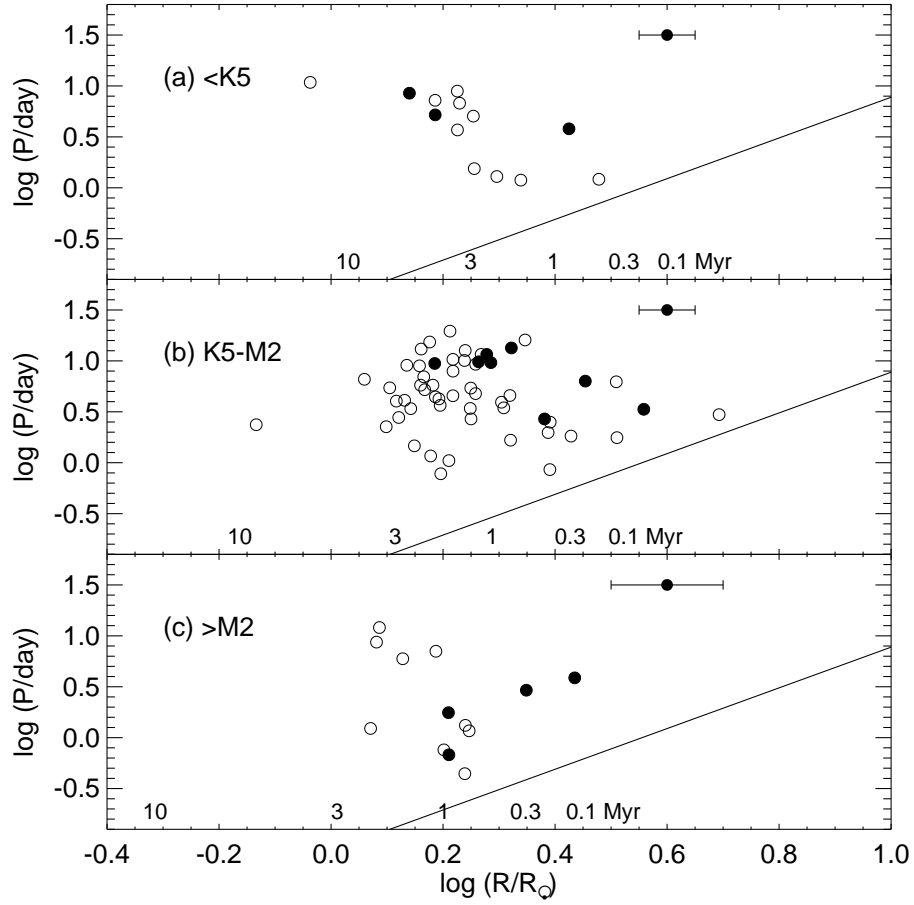


Fig. 5.— Period vs. radius for stars in NGC 2264. (a) stars with types K5 and earlier; (b) stars with types K5-M2; (c) stars with types M3 and later. Open circles are stars without $I_C - K_s$ excesses (i.e. without disks) and solid circles are stars with excesses (i.e. with disks). Typical standard error bars for each type range are indicated. The line in each panel indicates the slope expected if stellar angular momentum is conserved.

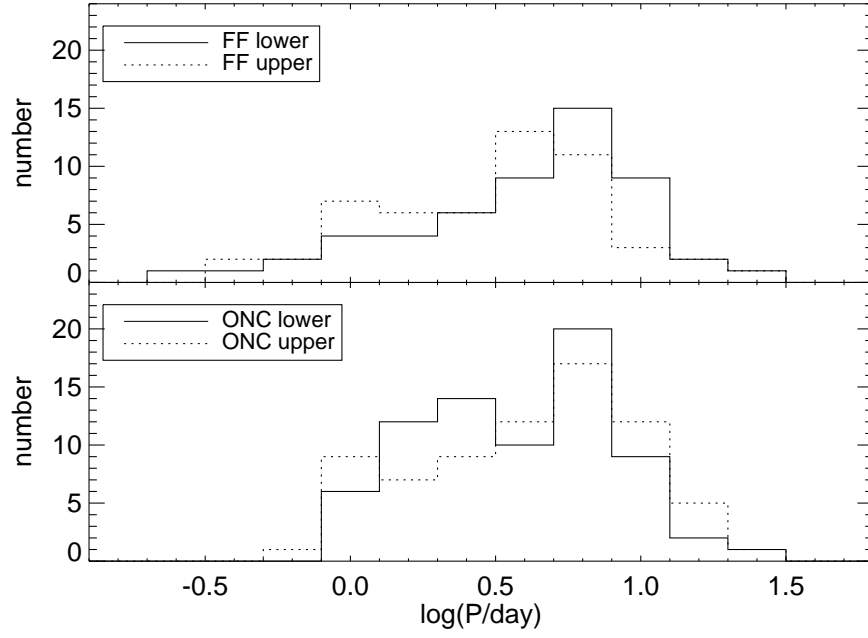


Fig. 6.— Histograms of distributions of periods for stars in (a) the FF and (b) the ONC for the upper and lower quartiles in radius. There is no difference in the period distributions. See Table 3 for $\langle \log P \rangle$, and $\langle \log R \rangle$.

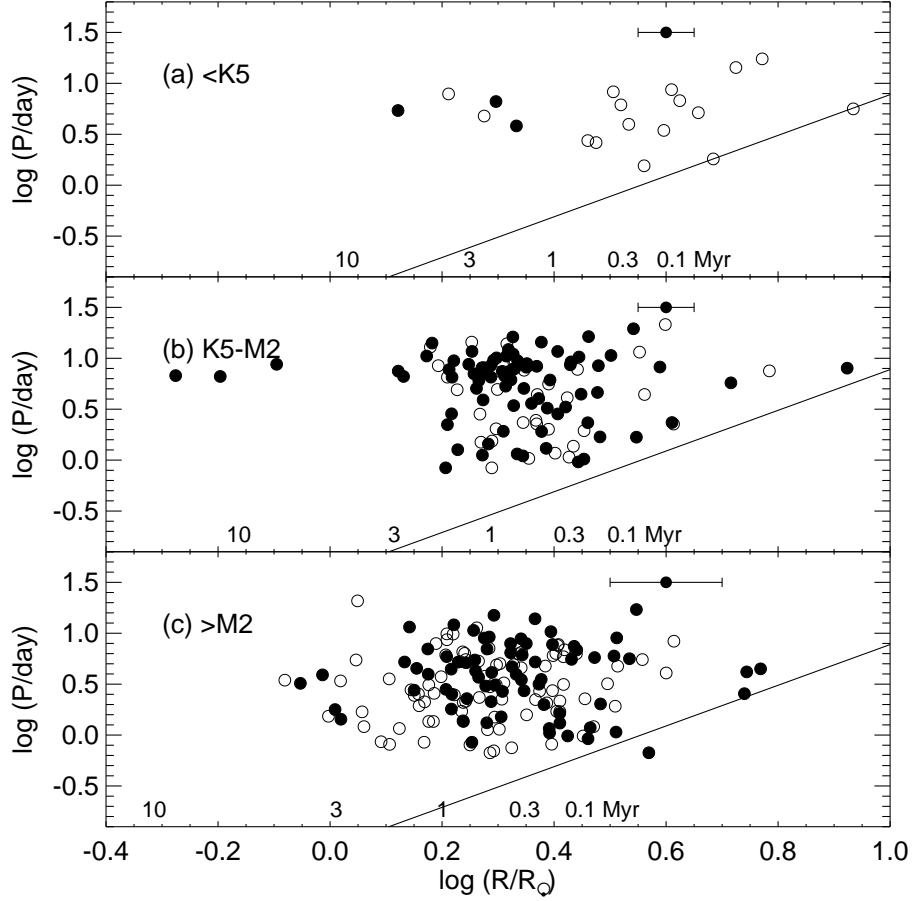


Fig. 7.— Period vs. radius for stars from the ONC, defined as the region covered by H97, periods taken from HRHC, SMMV, R01, CHS, and HBJM. (a) stars with types K5 and earlier; (b) stars with types K5-M2; (c) stars with types M3 and later. Open circles are stars without $I_C - K_s$ excesses (i.e. without disks) and solid circles are stars with excesses (i.e. with disks). Typical standard error bars for each type range are indicated. The line in each panel indicates the slope expected if stellar angular momentum is conserved.

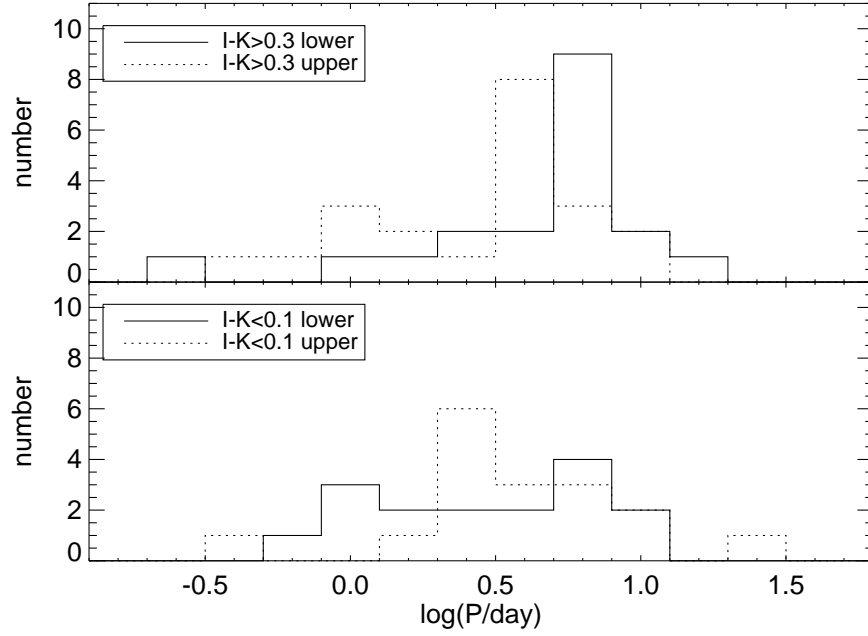


Fig. 8.— Histograms of distributions of periods for stars in the FF with (a) $I_C - K_s$ excess > 0.3 mag and (b) < 0.1 mag. There is no difference in the period distributions. See Table 3 for $\langle \log P \rangle$, and $\langle \log R \rangle$.

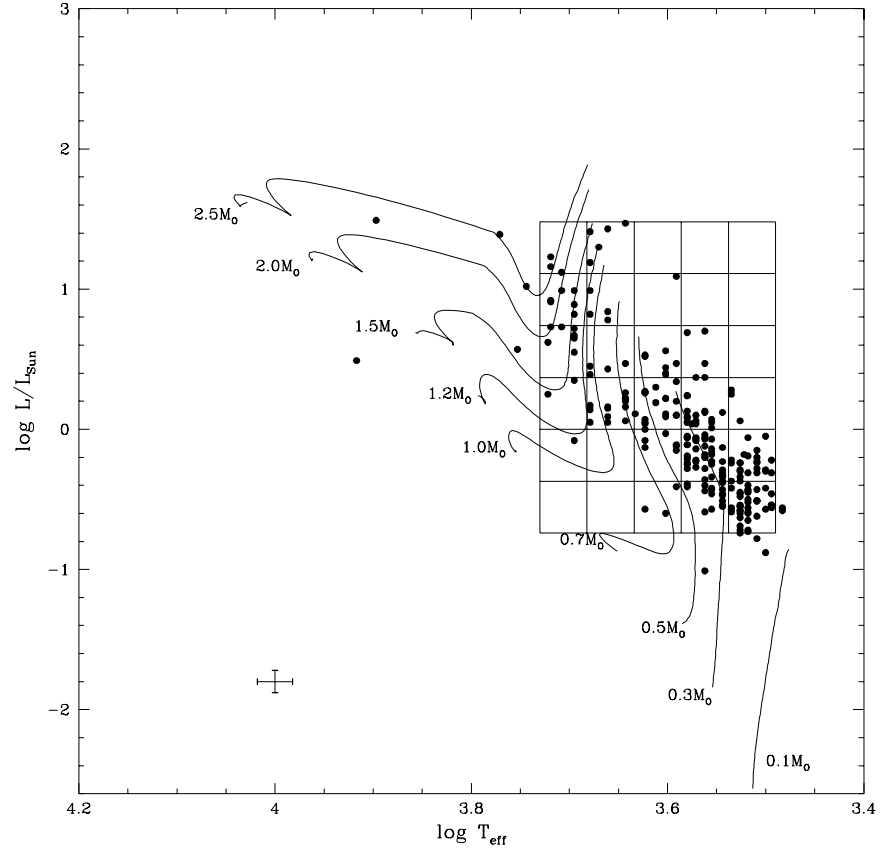


Fig. 9.— The HRD for the ONC stars. The evolutionary tracks are from D’Antona and Mazzitelli (1994). The grid shows the bins in the $\log L_{\text{bol}}$ and $\log T_{\text{eff}}$ plane into which we sorted the stars in order to look for trends in $\langle v \sin i \rangle$ with decreasing luminosity and increasing age. The estimated error bars for $\log L_{\text{bol}}$ and $\log T_{\text{eff}}$ are given in the lower left corner of the plot.

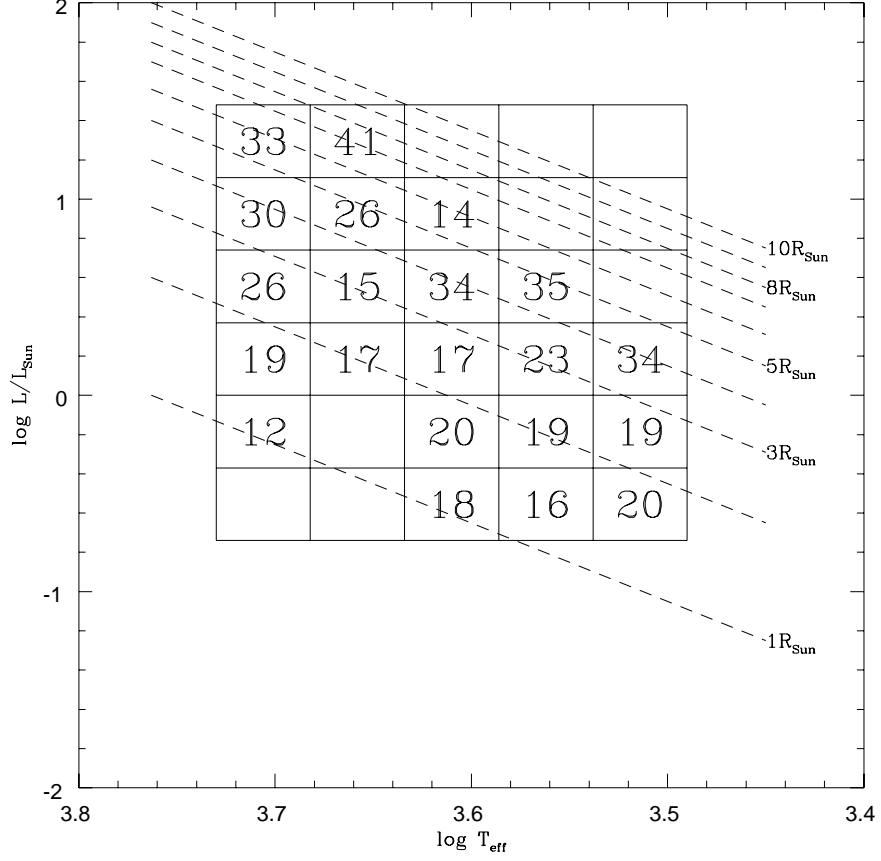


Fig. 10.— The values of $\langle v \sin i \rangle$ in km s^{-1} as a function of position in the $\log L_{\text{bol}}$ and $\log T_{\text{eff}}$ plane. Lines of constant radius are shown as dashed lines. Note that the trend in all columns is toward decreasing $\langle v \sin i \rangle$ with decreasing luminosity and decreasing radius, which indicates that angular momentum must be lost as stars evolve down their convective tracks. Table 4 indicates how many stars fall within each box in the grid and gives the statistical errors in the values of $\langle v \sin i \rangle$. Note that there is only one star in the top box in the middle column.

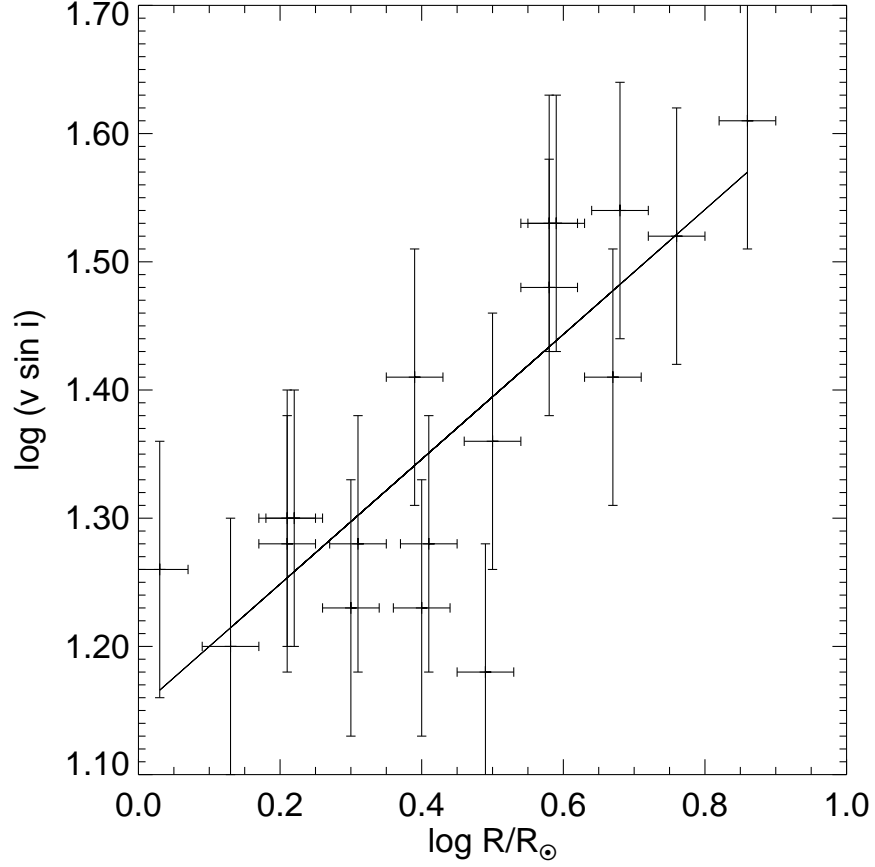


Fig. 11.— Mean values of $v \sin i$ and $\log R$ for each of the $(T_{\text{eff}}, L_{\text{bol}})$ ‘boxes’ from the previous plots. Note from previous figures that $\langle v \sin i \rangle$ is nearly constant along lines of constant R , thus encouraging us to combine the data for stars of all masses spanned by the RHM sample. The linear fit indicated here is $\log \langle v \sin i \rangle = 0.49(\pm 0.11) \log \langle R \rangle + 1.15(\pm 0.05)$.